Pergamon

Acta mater. Vol. 47, No. 1, pp. 219–233, 1999

Printed in Great Britain
PII: S1359-6454(98)00314-0
1359-6454/99 $19.00 + 0.00

CONTINUUM MODELING OF STRAIN-INDUCED MARTENSITIC TRANSFORMATION AT SHEAR-BAND INTERSECTIONS

V.I. LEVITAS[1]†, A.V. IDESMAN[1] and G.B. OLSON[2]

[1]Institute of Structural and Computational Mechanics, University of Hannover, Appelstrasse 9A, 30167 Hannover, Germany and [2]Department Materials Science and Engineering, Northwestern University, 2225 North Campus Drive, Evanston, IL 60208-3108, U.S.A.

(Received 10 March 1998; accepted 2 September 1998)

Abstract—A mesoscopic continuum thermomechanical approach is applied to the problem of strain-induced martensitic transformation at shear-band intersection. A computed transformation work functional combined with a critical driving force criterion and stability analysis are employed in the solution of boundary-value problems addressing aspects of martensitic transformations in a heterogeneous plastically deforming medium. Under boundary displacement control, solutions demonstrate preferred transformation at shear-band intersections, restricted growth beyond intersections, preferred transformation during rather than after intersection process, and sequential rather than simultaneous operation of multiple intersections of identical potency. Further growth beyond intersections is favored under fixed stress boundary conditions. Mesoscopic thermomechanical considerations offer useful insights into transformation behavior in a plastic environment. © *1998 Acta Metallurgica Inc. Published by Elsevier Science Ltd. All rights reserved.*

1. INTRODUCTION

There are many aspects of the interaction of martensitic phase transformations (PT) with plastic strain. We will concentrate in this paper on strain-induced PT in TRIP steels. It is known from experiments [1, 2] such as the electron microscopy observation in Fig. 1 [3] that

- shear-band intersections are the major nucleation sites;
- growth beyond the intersection region is generally very restricted;
- transformation occurs during the intersection events;
- transformation does not occur at every shear-band intersection.

There are microscopic models [1] which explain nucleation at shear-band intersection using some dislocation reactions. This approach has been used [3, 4] to develop a statistical macroscopic model for the prediction of PT kinetics and stress–strain relations. The fact that nucleation does not occur at every shear-band intersection is explained by varying potency of each intersection, i.e. by a distribution of shear-band thickness.

Recently a mesoscopic continuum thermomechanical theory of martensitic PT in inelastic materials has been developed [5–7]. Analytical and numerical solutions of several boundary-value problems were found using this theory [6, 8–10]. It appears that a number of experimental results related to interaction of plastic strain and PT can be explained, based on this theory and the solutions obtained. As an example, PT under compression of materials in Bridgman anvils and additional plastic shear due to rotation of one anvil was studied [6]. It was found that an enhancement of PT conditions due to a rotation of an anvil is attributed not to the plastic strain, but to the possibility of an additional displacement, compensating a transformation volume decrease. It is connected with a reduction of frictional shear stress in a radial direction due to the anvil rotation.

Another PT problem of a thin layer in a rigid-plastic half-space under the action of applied pressure and shear stresses is solved in [6]. This problem models PT due to the friction in the neighborhood of a contact surface or in a shear band.

These solutions illustrate the fundamental difference in PT conditions for a strongly nonhomogeneous pressure distribution in the first problem and for homogeneously distributed pressure and shear stresses in the second problem. In particular, rotation of an anvil in the first problem works much more effectively for the synthesis of strong phases than weak ones. In the second problem, additional shearing significantly improves the condition of appearance of soft materials and weakly affects the appearance of strong materials. Shear stresses and strains can render the PT *impossible*, if a PT criterion is violated due to the necessity of fulfillment of the yield condition for the parent phase. Consequently each experimental situation should be simulated carefully before any conclusion is made.

†To whom all correspondence should be addressed.

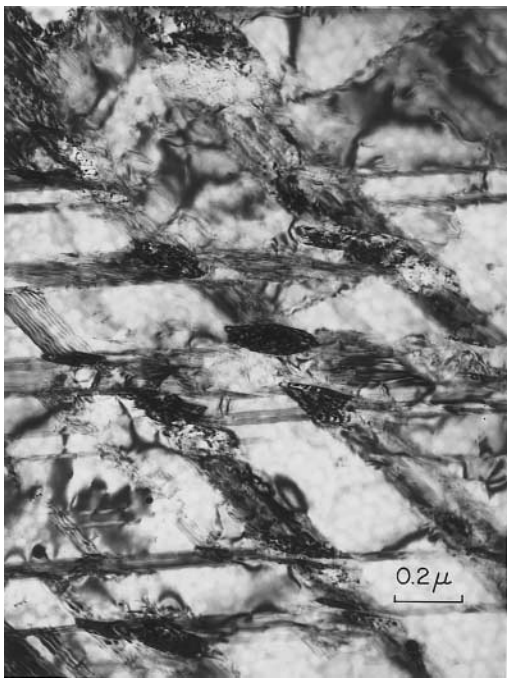

Fig. 1. Bright field transmission electron micrograph showing martensitic particle (dark) formed at shear-band intersections in cold-worked 301 stainless steel (from [3]).

The transformation condition in this mesoscopic theory includes (in contrast to previous approaches) the history of local stress variation in a volume during the transformation process. This appears to be very important for an explanation of experiments in the Bridgman anvils.

The aim of the present paper is to describe the experimental results on nucleation at shear-band intersection based on the mesoscopic continuum thermodynamic theory [5–7] and the solution of corresponding boundary-value problems with minimal assumption concerning the microscopic mechanism of transformation.

In Section 2 a problem formulation for martensitic PT in elastoplastic materials at finite strains is presented. We consider finite plastic and transformation strains and small elastic deformations. The deformation model is based on the multiplicative decomposition of the total deformation gradient into elastic, transformation and plastic parts, and the generalization of Prandtl–Reuss equations to the case of large strains and PT. The constitutive equations are then given in a rate form which is convenient for our numerical algorithm. The structure of equations is similar for the cases of small and large strains. Transformation strains can be treated like thermal strains in the numerical approach [11]. A transformation criterion and extremum principle for determination of location and volume of transformed region are presented.

The finite element solution algorithm, briefly discussed in Section 3, is realized in a step-by-step form with a variable actual configuration, i.e. equilibrium, kinematic and physical equations in actual configuration are used in the calculations.

In Section 4 the problem of transformation at shear-band intersection is formulated, solved and analyzed. It appears that all four aforementioned experimental peculiarities can be explained (at least qualitatively) in the framework of the continuum thermodynamic theory [5–7]. The key point of explanation is related to allowing for different stress variations in a transforming particle for different PT scenarios. Actual solutions obtained with the help of our extremum principle describe the experimental results.

Direct tensor notations are used throughout this paper. Vectors and tensors are denoted in boldface type; $\mathbf{A}\cdot\mathbf{B}$ and $\mathbf{A}:\mathbf{B}$ are the contraction of tensors over one and two indices. Let a superscript t and -1 denote transposed and inverse operation; subscripts s and à designate symmetrical and antisymmetrical tensor parts; $\mathbf{I}$ is the unit tensor; *dev* $\mathbf{A}$ is a deviatoric part of $\mathbf{A}$; $:=$means equals per definition; a point above indicates the material time derivative.

2. PROBLEM FORMULATION

PT is modeled here as the thermomechanical process of growth of a transformation deformation gradient from unit tensor $\mathbf{I}$ to a final value which is accompanied by a change of mechanical and thermal material properties.

2.1. Kinematics

Let the motion of the uniformly deformed infinitesimal neighborhood of a material point in a process of martensitic PT be described by the function $\mathbf{r} = \mathbf{r}(\mathbf{r}_\tau, t)$, where $\mathbf{r}$ and $\mathbf{r}_\tau$ are the positions of points in the actual V and the reference V_τ configurations, t is the time. We neglect thermal strains (they are small with respect to transformation strains) and assume for the finite strains a multiplicative decomposition of the total deformation gradient $\mathbf{F} = \partial\mathbf{r}/\partial\mathbf{r}_\tau$ into elastic $\mathbf{F}_e$, transformational $\mathbf{F}_t$ and plastic (symmetrical) $\mathbf{U}_p$ parts [5, 8], i.e.

$$\mathbf{F} = \mathbf{F}_e \cdot \mathbf{F}_t \cdot \mathbf{U}_p = \mathbf{V}_e \cdot \mathbf{R}_e \cdot \mathbf{F}_t \cdot \mathbf{U}_p \qquad (1)$$

where $\mathbf{F}_e = \mathbf{V}_e \cdot \mathbf{R}_e$, $\mathbf{V}_e$ is the symmetrical elastic left stretch tensor, $\mathbf{R}_e$ is the rotation tensor. Let us introduce the internal dimensionless order parameter $\xi (0 \leqslant \xi \leqslant 1)$ which is related to $\mathbf{F}_t$ and has the following properties: PT starts at $\xi = 0$ and finishes at $\xi = 1$; when ξ varies between 0 and 1, the transformation strain grows from 0 to maximum value $\mathbf{F}_{t\ max}$. We can thus define the order parameter as $\xi := |\mathbf{F}_t - \mathbf{I}| / |\mathbf{F}_{t\ max} - \mathbf{I}|$. When solving the elastoplastic problem, the rate form of equation (1), derived by differentiation with respect

to time, is used. The velocity gradient **l** and deformation rate **d** are described as follows:

Box 1. Problem formulation

1. Kinematics

A multiplicative decomposition of the total deformation gradient **F**

$$\mathbf{F} := \frac{\partial \mathbf{r}}{\partial \mathbf{r}_\tau} = \mathbf{F}_e \cdot \mathbf{F}_t \cdot \mathbf{U}_p = \mathbf{V}_e \cdot \mathbf{R}_e \cdot \mathbf{F}_t \cdot \mathbf{U}_p. \quad (2)$$

Decomposition of the total deformation rate **d**

$$\mathbf{d} := \left(\frac{\partial \mathbf{v}}{\partial \mathbf{r}}\right)_s = \overset{\triangle}{\mathbf{B}}_e + \mathbf{d}_t + \mathbf{d}_D, \quad (3)$$

$$\mathbf{d}_D := (\mathbf{R}_e \cdot \mathbf{F}_t \cdot \dot{\mathbf{U}}_p \cdot \mathbf{U}_p^{-1} \cdot \mathbf{F}_t^{-1} \cdot \mathbf{R}_e^t)_s,$$
$$\mathbf{d}_t := (\mathbf{V}_e \cdot \mathbf{R}_e \cdot \dot{\mathbf{F}}_t \cdot \mathbf{F}_t^{-1} \cdot \mathbf{R}_e^t \cdot \mathbf{V}_e^{-1})_s, \quad (4)$$

$$\overset{\triangle}{\mathbf{B}}_e := \dot{\mathbf{B}}_e + \mathbf{B}_e \cdot \bar{\mathbf{W}} + \bar{\mathbf{W}}^t \cdot \mathbf{B}_e,$$
$$\bar{\mathbf{W}} = \mathbf{W} - (\mathbf{R}_e \cdot \dot{\mathbf{F}}_t \cdot \mathbf{F}_t^{-1} \cdot \mathbf{R}_e^t \cdot)_a,$$
$$\mathbf{W} = \left(\frac{\partial \mathbf{v}}{\partial \mathbf{r}}\right)_a,$$
$$\mathbf{B}_e := 0.5\,(\mathbf{V}_e \cdot \mathbf{V}_e - \mathbf{I}) \approx \mathbf{V}_e - \mathbf{I} \ll \mathbf{I}. \quad (5)$$

2. Constitutive equations

Elastic Hooke's law

$$\mathbf{T} = \mathbf{E}(\xi) : \mathbf{B}_e = \lambda(\xi) I_1(\mathbf{B}_e)\mathbf{I} + 2\mu(\xi)\,\mathbf{B}_e. \quad (6)$$

Yield function

$$f(\mathbf{T}, q, \xi) = \sigma_i - \sigma_y(q, \xi) \leqslant 0, \quad \dot{q} = (2/3\,\mathbf{d}_D : \mathbf{d}_D)^{1/2}. \quad (7)$$

In an elastic region

$$f < 0 \text{ or } f = 0, \qquad \frac{\partial f}{\partial \mathbf{T}} : \overset{\triangle}{\mathbf{T}} + \frac{\partial f}{\partial \xi}\dot{\xi} \leqslant 0, \quad (8)$$

$$\overset{\triangle}{\mathbf{T}} = \mathbf{E} : (\mathbf{d} - \mathbf{d}_t) + \frac{\partial \mathbf{E}}{\partial \xi} : \mathbf{B}_e\,\dot{\xi}. \quad (9)$$

In an elastoplastic region

$$f = 0, \qquad \frac{\partial f}{\partial \mathbf{T}} : \overset{\triangle}{\mathbf{T}} + \frac{\partial f}{\partial \xi}\dot{\xi} > 0. \quad (10)$$

Plastic flow rule

$$\mathbf{d}_D = \lambda_1 \mathbf{s}, \qquad \lambda_1 \geq 0 \Longrightarrow \quad (11)$$

$$\overset{\triangle}{\mathbf{T}} = \left(\mathbf{E} - \frac{1}{\nu}\mathbf{E} : \mathbf{s}\frac{\partial f}{\partial \mathbf{T}} : \mathbf{E}\right) : (\mathbf{d} - \mathbf{d}_t) + \frac{\partial \mathbf{E}}{\partial \xi} : \mathbf{B}_e\,\dot{\xi} - \frac{1}{\nu}\left(\frac{\partial f}{\partial \mathbf{T}} : \frac{\partial \mathbf{E}}{\partial \xi} : \mathbf{B}_e\,\dot{\xi} + \frac{\partial f}{\partial \xi}\dot{\xi}\right)\mathbf{E} : \mathbf{s}, \quad (12)$$

$$\nu = \frac{\partial f}{\partial \mathbf{T}} : \mathbf{E} : \mathbf{s} - \frac{\partial f}{\partial q}\left(\frac{2}{3}\mathbf{s} : \mathbf{s}\right)^{1/2}, \quad (13)$$

$$\mathbf{d}_D = \frac{1}{\nu}\left[\frac{\partial f}{\partial \mathbf{T}} : \mathbf{E} : (\mathbf{d} - \mathbf{d}_t) + \frac{\partial f}{\partial \mathbf{T}} : \frac{\partial \mathbf{E}}{\partial \xi} : \mathbf{B}_e\,\dot{\xi} + \frac{\partial f}{\partial \xi}\dot{\xi}\right]\mathbf{s}. \quad (14)$$

3. Equilibrium equations for neglected body forces

$$\nabla \cdot \mathbf{T} = 0 \quad (15)$$

4. PT criterion

$$\bar{X} := \frac{1}{m_n}\int_{V_n}\int_0^1 \mathbf{T} : \mathbf{d}_t\,\frac{\partial t}{\partial \xi}\mathrm{d}\,\xi\,\mathrm{d}V_n - (\psi_2^\theta - \psi_1^\theta) = k_c, \quad (16)$$

$$m_n = \int_{V_n} \rho\,\mathrm{d}V_n,$$

$$\bar{X} := k_c, \quad \Longrightarrow \quad \text{PT occurs.} \quad (17)$$

5. Extremum principle for PT

$$\bar{X}(V^*) - k_c < 0 = \bar{X}(V) - k_c \quad (18)$$

or

$$\varphi(V^*) \rightarrow \max, \quad \varphi := \frac{1}{m_n}\int_{V_n}\int_0^1 \mathbf{T} : \mathbf{d}_t\,\frac{\partial t}{\partial \xi}\mathrm{d}\,\xi\,\mathrm{d}V_n. \quad (19)$$

6. Extremum principle for determination of stable solution (global PT criterion)

$$\int_S \int_{\mathbf{u}_1}^{\mathbf{u}_2} \mathbf{p} \cdot \mathrm{d}\,\mathbf{u}\,\mathrm{d}\,S \rightarrow \min$$

(particular case at prescribed **u** at S). (20)

$$\mathbf{l} := \frac{\partial \mathbf{v}}{\partial \mathbf{r}} = \dot{\mathbf{F}} \cdot \mathbf{F}^{-1} = \dot{\mathbf{F}}_e \cdot \mathbf{F}_e^{-1} + \mathbf{F}_e \cdot \dot{\mathbf{F}}_t \cdot \mathbf{F}_t^{-1} \cdot \mathbf{F}_e^{-1} + \mathbf{F}_e \cdot \mathbf{F}_t \cdot \dot{\mathbf{U}}_p \cdot \mathbf{U}_p^{-1} \cdot \mathbf{F}_t^{-1} \cdot \mathbf{F}_e^{-1} = \left(\dot{\mathbf{V}}_e \cdot \mathbf{V}_e^{-1} + \mathbf{V}_e \cdot \Omega \cdot \mathbf{V}_e^{-1}\right) + \mathbf{V}_e \cdot \mathbf{R}_e \cdot \dot{\mathbf{F}}_t \cdot \mathbf{F}_t^{-1} \cdot \mathbf{R}_e^t \cdot \mathbf{V}_e^{-1} + \mathbf{V}_e \cdot \mathbf{R}_e \cdot \mathbf{F}_t \cdot \dot{\mathbf{U}}_p \cdot \mathbf{U}_p^{-1} \cdot \mathbf{F}_t^{-1} \cdot \mathbf{R}_e^t \cdot \mathbf{V}_e^{-1}, \quad (21)$$

$$\mathbf{d} := (\mathbf{l})_s = \mathbf{V}_e^{-1} \cdot \mathring{\mathbf{B}}_e \cdot \mathbf{V}_e^{-1} + \left(\mathbf{V}_e \cdot \mathbf{Q} \cdot \mathbf{V}_e^{-1}\right)_s + \left(\mathbf{V}_e \cdot \mathbf{R}_e \cdot \dot{\mathbf{F}}_t \cdot \mathbf{F}_t^{-1} \cdot \mathbf{R}_e^t \cdot \mathbf{V}_e^{-1}\right)_s, \quad (22)$$

where $\mathbf{B}_e := 0.5\,(\mathbf{F}_e \cdot \mathbf{F}_e^t - \mathbf{I}) = 0.5\,(\mathbf{V}_e \cdot \mathbf{V}_e - \mathbf{I})$ is the elastic strain tensor, $\mathbf{v} = \dot{\mathbf{r}}$ is the velocity vector, $\mathbf{Q} := \mathbf{R}_e \cdot \mathbf{F}_t \cdot \dot{\mathbf{U}}_p \cdot \mathbf{U}_p^{-1} \cdot \mathbf{F}_t^{-1} \cdot \mathbf{R}_e^t$, $\mathring{\mathbf{B}}_e := \dot{\mathbf{B}}_e + \mathbf{B}_e \cdot \Omega + \Omega^t \cdot \mathbf{B}_e$ is called the R-derivative associated with the skew-symmetric spin tensor $\Omega = \dot{\mathbf{R}}_e \cdot \mathbf{R}_e^t$, we used relation $\mathbf{V}_e^{-1} \cdot \mathring{\mathbf{B}}_e \cdot \mathbf{V}_e^{-1} = (\dot{\mathbf{V}}_e \cdot \mathbf{V}_e^{-1} + \mathbf{V}_e \cdot \Omega \cdot \mathbf{V}_e^{-1})_s$ which can be checked by direct calculations, see [12].

We assume that the elastic strains are small, i.e. $\mathbf{V}_e = \mathbf{I} + \boldsymbol{\varepsilon}$, $\boldsymbol{\varepsilon} \ll \mathbf{I}$, $\mathbf{V}_e^{-1} = \mathbf{I} - \boldsymbol{\varepsilon}$, $\mathbf{B}_e = \boldsymbol{\varepsilon}$. Then we have from equation (21)

$$\boldsymbol{\Omega} = \mathbf{W} - \left(\mathbf{R}_e \cdot \dot{\mathbf{F}}_t \cdot \mathbf{F}_t^{-1} \cdot \mathbf{R}_e^t\right)_a - (\mathbf{Q})_a, \quad (23)$$

where $\mathbf{W} = (\mathbf{l})_a$ is the spin tensor. Substituting (23) into (22) for $\mathring{\mathbf{B}}_e$ and allowing for $(\boldsymbol{\varepsilon} \cdot \mathbf{Q} + \mathbf{Q}^t \cdot \boldsymbol{\varepsilon})_s \ll (\mathbf{Q})_s$ we get the kinematic equations presented in Box 1 where $\mathbf{d}$, $\mathbf{d}_t$, $\mathbf{d}_D$ are the rates of the total, transformational and dissipative (due to plastic strain) deformations, respectively; $I_1(\mathbf{B}_e)$ is the first invariant of $\mathbf{B}_e$; $\overset{\triangle}{\mathbf{C}} := \dot{\mathbf{C}} + \mathbf{C} \cdot \bar{\mathbf{W}} + \bar{\mathbf{W}}^t \cdot \mathbf{C}$ is the objective derivative associated with tensor $\bar{\mathbf{W}}$. Before PT we have $\mathbf{F}_t = \mathbf{I}$, and the rate form of the kinematic equation (3) yields

$$\mathbf{d} = \overset{\triangle}{\mathbf{B}}_e + \mathbf{d}_p, \quad \mathbf{d}_p = \left(\mathbf{R}_e \cdot \dot{\mathbf{U}}_p \cdot \mathbf{U}_p^{-1} \cdot \mathbf{R}_e^t\right)_s,$$

where $\overset{\triangle}{\mathbf{B}}_e := \dot{\mathbf{B}}_e + \mathbf{B}_e \cdot \mathbf{W} + \mathbf{W}^t \cdot \mathbf{B}_e$ is the objective Jaumann derivative of the tensor $\mathbf{B}_e$.

At small plastic strains before completion of PT $\mathbf{U}_p = \mathbf{I} + \boldsymbol{\varepsilon}_p$, $\boldsymbol{\varepsilon}_p \ll \mathbf{I}$ we get from (1) that $\mathbf{V}_e \cdot \mathbf{R}_e \approx \mathbf{R}_e = \mathbf{F} \cdot \mathbf{F}_t^{-1}$ and $\mathbf{d}_t = (\mathbf{F} \cdot \mathbf{F}_t^{-1} \cdot \dot{\mathbf{F}}_t \cdot \mathbf{F}^{-1})_s$, $\bar{\mathbf{W}} = \mathbf{W} - (\mathbf{F} \cdot \mathbf{F}_t^{-1} \cdot \dot{\mathbf{F}}_t \cdot \mathbf{F}^{-1})_a$.

2.1. Constitutive equations for elastoplasticity at finite strains

We use the generalization of the Prandtl–Reuss equations to the case of large strains for isotropic elastoplastic materials with isotropic hardening [11, 12]. The relationships during PT are presented in Box 1. Here $\mathbf{T}$ is the Cauchy stress tensor; q is the accumulated plastic strain; $\sigma_i = (3/2\,\mathbf{s}:\mathbf{s})^{1/2}$ is the stress intensity; $\mathbf{s} = dev\mathbf{T}$ is the deviatoric Cauchy stress tensor; $\sigma_y(q,\xi)$ is the yield stress function to be found experimentally, $\mathbf{E}(\xi)$ is the elastic modulus tensor; $\lambda(\xi)$, $\mu(\xi)$ are the Lame coefficients which depend on ξ. Equation (9) is the rate form of equation (6) (see [11, 12]). It is necessary here to make some comments.

(1) From the second law of thermodynamics for small elastic strains we derive $\mathbf{T} = \rho(\partial\psi/\partial\mathbf{B}_e)$ [ψ is this the specific Helmholtz free energy, $\rho = \rho(\xi) = \rho_1 det\mathbf{F}(\xi)$ is the mass density during PT, ρ_1 is the mass density at $\xi = 0$, i.e. before PT]. We assume that

$$\psi(\mathbf{B}_e, \theta, \xi) = \frac{\mathbf{B}_e : \mathbf{E}(\xi) : \mathbf{B}_e}{2\rho(\xi)} + \psi^\theta(\theta, \xi), \quad (24)$$

where ψ^θ is the thermal part of the specific Helmholtz free energy.

Then we obtain Hooke's law (6).

(2) Computational algorithms do not usually involve equation (11) as such, but the quasi-linear relationship between the stress rate and the rate of deformation. Using equations (3), (6) and (11) and the loading condition $\dot{f} = 0$ we get equations (12) and (14) (see [11, 12]). Before PT, $\mathbf{d}_D = \mathbf{d}_p = (\mathbf{R}_e \cdot \dot{\mathbf{U}}_p \cdot \mathbf{U}_p^{-1} \cdot \mathbf{R}_e^t)_s$ holds, and equation (12) has the form

$$\overset{\triangle}{\mathbf{T}} = \left(\mathbf{E} - \frac{1}{\nu}\mathbf{E} : \mathbf{s}\frac{\partial f}{\partial \mathbf{T}} : \mathbf{E}\right) : \mathbf{d}, \quad (25)$$

where in equations (7)–(10) we should take into account that f and $\mathbf{E}$ do not depend on ξ.

(3) The tensor $\overset{\triangle}{\mathbf{T}}$ which appears in relationships (8) and (10) can be replaced by tensor $\dot{\mathbf{T}}$, since for the accepted expressions (7) for $\dot{f}$, the relation $(\partial f/\partial \mathbf{T}) : \overset{\triangle}{\mathbf{T}} = (\partial f/\partial \mathbf{T}) : \dot{\mathbf{T}}$ is valid. However, for calculations it is convenient to write relationships (8) and (10) in terms of $\overset{\triangle}{\mathbf{T}}$.

2.2 Mesoscopic transformation criterion

The transformation criterion is consisted with the second law of thermodynamic and has the following form [5, 7]

$$\int_{V_n} X \mathrm{d}V_n := \int_{V_n} \int_0^1 \frac{\rho_1}{\rho(\xi)} \mathbf{T} : \mathbf{d} \frac{\partial t}{\partial \xi} \mathrm{d}\xi \mathrm{d}V_n - \int_{V_n} \int_0^1 \frac{\rho_1}{\rho(\xi)} \mathbf{T} : \mathbf{d}_D \frac{\partial t}{\partial \xi} \mathrm{d}\xi \mathrm{d}V_n - \int_{V_n} \rho_1(\psi_2 - \psi_1)\mathrm{d}V_n = \int_{V_n} \rho_1 k_c \mathrm{d}V_n + \int_\Sigma \gamma \mathrm{d}\Sigma. \quad (26)$$

Here X is the local dissipation increment (driving force) in the course of PT due to PT only (excluding plastic and other types of dissipation); $\int_{V_n} \int_0^1 (\rho_1/\rho(\xi))\mathbf{T} : \mathbf{d}_D \mathrm{d}\xi \mathrm{d}V_n$ is the local dissipation

increment in the course of PT due to plastic deformation only; ψ_2, ψ_1 are the specific Helmholtz free energies for the second (after PT, $\xi = 1$) and the first (before PT, $\xi = 0$) phase; V_n is the volume of transforming particle at $\xi = 0$ (before PT); k_c is an experimentally determined critical value of dissipation for PT which can depend on other parameters, e.g. θ, $\mathbf{U}_p$; Σ is the surface of transformed region after the finishing of PT and γ is the surface energy per unit area after the PT. Energy per unit area is an idealization of energy per unit volume due to very nonhomogeneous strain distribution in a thin layer. Below, for our numerical implementation, we study the transforming regions with the same volume and surface (excepting one example), therefore the surface energy is constant and we neglect it.

Let us consider some simplifications. We assume that

$$\psi_i(\mathbf{B}_e, \theta, \rho) = \frac{\mathbf{B}_e : \mathbf{E}_i : \mathbf{B}_e}{2\rho_i} + \psi_i^{\theta}(\theta), \qquad (27)$$

$i = 1,2$ correspond to the value before PT at $\xi = 0$ and after PT at $\xi = 1$, respectively, $\Delta\psi^{\theta} = \psi^{\theta}{}_2 - \psi^{\theta}{}_1$ defines the chemical driving force. In the case if

(a) the phases have the same elastic properties $\mathbf{E}(\xi) = \mathbf{E}_1 = \mathbf{E}_2 = \text{const}$;
(b) $\rho(\xi) \approx \rho = \text{const}$, i.e. transformation volumetric strain is small (elastic strains are small, plastic strains due to incompressibility do not change mass density);
(c) θ and k are homogeneous in the transforming volume;

then equation (26) can be transformed into equation (16), where $\bar{X}$ is the driving force for nucleation (averaged over the transforming volume), m_n is the transforming particle mass. Here we take into account equation (3) and the condition that $(1/\rho(\xi))\mathbf{T} : \overset{\triangle}{\mathbf{B}}_e = (1/\rho(\xi))\mathbf{T} : \dot{\mathbf{B}}_e$ and for small elastic strains $\mathbf{T} = \rho(\xi)(\partial\psi/\partial\mathbf{B}_e)$.

Equation (16) is a final form of the PT criterion which is used in the present paper. Such a formulation is similar to the introduction of a yield condition, e.g. equation $(7)_1$. The formal way of derivation of the criterion (16) is the following. If PT and plastic flow in the given material point are thermodynamically independent, then at $\bar{X} < 0$ the PT is impossible (contradicts to the second law of thermodynamics). At $\bar{X} = 0$ the PT is possible, but it will be PT without dissipation due to PT. Since usually rather large dissipation accompanies PT, we assume that the calculated increment $\bar{X}$ of dissipation due to PT reaches the experimentally determined value k. From the other side, the criterion can be justified in an approximate way by the microscopic Olson–Cohen dislocation dissociation model of martensitic nucleation [13, 14]. By this mechanism, nucleation occurs in a volume of thickness t by the passage of a transformation dislocation through the volume. The critical net driving force [$\bar{X}$ of (16)] for this process is expressed by

$$\bar{X}_c = \frac{2\gamma}{t} + W_f, \qquad (28)$$

where γ is the nucleus interfacial energy and W_f is the frictional work of interfacial motion determined principally by solid solution hardening [15]. For the problem of microscopic shear-band intersection considered here, the transformed region can be treated as a nucleus with thickness t equal to the shear-band thickness. Fixing t then makes $\bar{X}_c$ a constant as assumed throughout this paper. This approximation neglects a contribution to W_f from forest dislocation hardening associated with plastic prestrain [16], which will be addressed in further studies. At the same time a mesoscopic continuum approach allows us to determine more precise an expression for the driving force $\bar{X}_c$, in particular its stress history dependence.

2.3. Extremum principle for PT

In a general case the position and volume V_n of a new transforming region in the PT criterion (26) or (16) for each increment of boundary conditions or temperature θ are unknown. To determine them, we can use the extremum principle (18) which follows from the postulate of realizability [6, 7, 17], where V_n and $V^*{}_n$ are the actual and possible volume of transformed particle. The physical interpretation of the principle (18) is as follows: as soon as for some region V_n the PT criterion (16) is fulfilled for the first time, PT occurs in V_n. For all other $V^*{}_n$ the inequality (18) is valid, because in the opposite case the PT criterion (16) will be met for this $V^*{}_n$ earlier than for V_n. As only the work integral φ in equation (18) depends on the volume V_n, the extremum principle (19) follows from principle (18).

It is possible that under the given increment of boundary conditions the local PT criterion (16) and extremum principle (18) allow several solutions, e.g. transformation in different places or propagation of different interfaces. At least two solutions are always possible: first, the solution without the PT, second, the solution with the PT. Such a situation was revealed in papers [8, 17]. It was suggested that the best unique solution among all possible is the stable one. To formulate the stability criterion again the *postulate of realizability* is applied. Using it, the extremum principle for the whole volume is derived to choose the stable solution. The general extremum principle [17] is too bulky. Here we will use the simplified version (20) of this principle at the prescribed displacements $\mathbf{u}$ at the boundary S of volume V, where $\mathbf{p}$ is the traction vector, and $\mathbf{u}_1$ and $\mathbf{u}_2$ correspond to the start and end of PT. It follows from principle (20) that the stable solution minimizes the work of external stresses. Consequently, the fulfillment of the local PT criterion is not enough for the occurrence of PT and

only the extremum principle (20) which represents the global PT criterion gives the final solution.

3. NUMERICAL METHOD

To define PT conditions using PT criterion (26) or (16) it is necessary to calculate the variation of local stress and strain distributions in a transformed volume as functions of growing transformation strain. For this purpose the isotropic elastoplastic problem at large strains with given transformation strain (which is prescribed incrementally) is solved numerically using FEM. Quadratic triangular finite elements are used. The kinematic and constitutive equations presented above are brought to such a form that we can use the solution algorithm briefly presented in the Appendix and described in detail in [11]. The solution is realized in step-by-step form, i.e. with a known solution at time t_n one should find a solution at time t_{n+1}, where n is the step number. A variable actual configuration is used, i.e. equilibrium, kinematic and constitutive equations in actual configuration are used in calculations. A constant or variable tangent stiffness matrix [K] (see [11]) or more efficiently a stiffness matrix based on the algorithmic tangent tensor [18] can be used, as the problem solution depends only indirectly on the type of [K] matrix defining the convergence rate of an iterative process.

Let us next consider a technique for preserving exact plastic volume. When we present the stress tensor as $\mathbf{T} = p\mathbf{I} + \mathbf{s}$ (p is pressure), then from equation (12) for $\overset{\triangle}{\mathbf{s}}$ we get

$$\overset{\triangle}{\mathbf{s}} = \mathbf{E} : (dev\ \mathbf{d} - dev\ \mathbf{d}_t) - \frac{1}{\nu}\mathbf{E} : \mathbf{s}\frac{\partial f}{\partial \mathbf{T}} : \mathbf{E} : (\mathbf{d} - \mathbf{d}_t) + \frac{\partial \mathbf{E}}{\partial \xi} : \bar{\mathbf{B}}_e\,\dot{\xi} - \frac{1}{\nu}\left(\frac{\partial f}{\partial \mathbf{T}} : \frac{\partial \mathbf{E}}{\partial \xi} : \mathbf{B}_e\,\dot{\xi} + \frac{\partial f}{\partial \xi}\dot{\xi}\right)\mathbf{E} : \mathbf{s}. \quad (29)$$

The value $\bar{\mathbf{B}}_e = dev\mathbf{B}_e = \mathbf{s}/2\mu$ [see equation (6)] is defined using known $\mathbf{s}$ during numerical integration of equation (29). The pressure p can be directly calculated from Hooke's law (6)

$$p = \left(\lambda(\xi) + \frac{2}{3}\mu(\xi)\right) I_1(\mathbf{B}_e), \quad (30)$$

as the value I_1 ($\mathbf{B}_e$) can be defined from equation (2) allowing for the condition of plastic incompressibility $det\mathbf{U}_p = \mathbf{I}$ and small elastic strain ($det\mathbf{V}_e = 1 + I_1(\mathbf{B}_e)$), i.e.

$$I_1(\mathbf{B}e) = (det\ \mathbf{F})/(det\ \mathbf{F}_t) - 1. \quad (31)$$

Use of equations (29)–(31) instead of equation (12) for calculation of the stress tensor $\mathbf{T}$ allows us to satisfy exactly the condition of plastic incompressibility, because numerical integration of equation (12) for p can accumulate errors.

The set of equations presented above have similar structures for the cases of small and large strains [the differences are in the use of $\overset{\triangle}{\mathbf{T}}$ in equation (12) and $\overset{\triangle}{\mathbf{B}}_e$ in equation (3) instead of $\dot{\mathbf{T}}$ and $\dot{\mathbf{B}}_e$ for the case of small strains]. For example, for small plastic strains in a transforming region, but finite transformation strains and finite plastic strains outside, we additionally need (compared with the case of small strains) to calculate the total gradient $\mathbf{F}$ and the spin tensor $\mathbf{W}$ only, which is very simple. We do not need the tensors $\mathbf{R}_e$, $\mathbf{U}_p$ because we use the rate form of kinematic (3) and constitutive equations. For finite plastic strains in the transforming region we should calculate $\dot{\mathbf{U}}_p$ from expression $(4)_1$ for $\mathbf{d}_D$; $\mathbf{d}_D$ is defined from equation (14). Then at time $t + dt$ we should compute $\mathbf{U}_p$ and using known values of $\mathbf{U}_p$, $\mathbf{F}$, $\mathbf{F}_t$, $\mathbf{V}_e$ define $\mathbf{R}_e$ from equation (1); $\mathbf{V}_e \approx \mathbf{I} + \mathbf{B}_e$ can be calculated from equations (31) and (6) when stresses $\mathbf{s}$ are known.

Here we consider a uniform temperature distribution. We do not need temperature to define the stress–strain state, but only for calculation of the thermal part of the specific Helmholtz free energy ψ_i^θ. In this paper the "inverse" problem is solved, i.e. the position and size of the transforming region are prescribed in advance, and then the condition for PT is defined. For example, when the stress–strain state is computed we can determine the temperature of PT from equation (26) or (16) [we can consider equation (26) or (16) as one scalar equation with respect to temperature]. The extremum principle in the form of equation (19) is used to analyze the solutions obtained.

4. FEM SOLUTION OF THE PROBLEM OF TRANSFORMATION AT A SHEAR-BAND INTERSECTION

Let us consider the thermomechanical formulation of a model problem of transformation at shear bands. We will neglect the precise physical mechanisms of inelastic deformation inside the shear band (e.g. formation of h.c.p. ε-martensite, mechanical twins, dense stacking-fault bundles and slip dislocation bands) and will describe plasticity in the framework of phenomenological flow theory. Strain localization at such a microscale is attributed not to softening, but to a heterogeneous defect distribution. We thus introduce a potential shear-band region in advance as a region where the material deforms elastoplastically (Fig. 2). Outside the shear bands material behaves elastically only, i.e. a very high yield stress is assumed. Neglecting the microscopic mechanisms means that all possible nucleation places differ by transformation work done during the nucleation events only. For each possible transformation place after calculation of transformation work corresponding transformation temperature can be found from PT criterion (26). Actual nucleation place corresponds to maximum transformation work (or maximum transformation temperature).

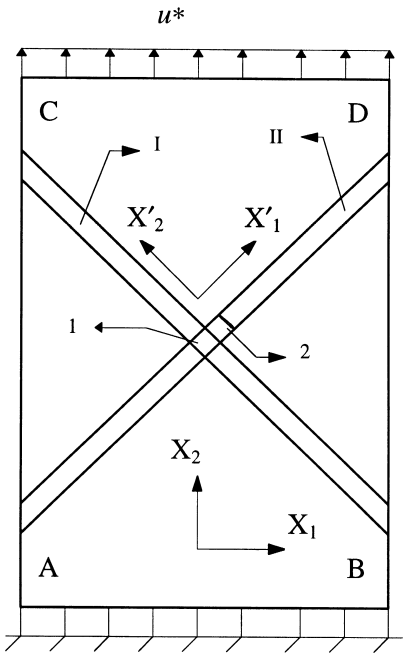

Fig. 2. Cross section of a sample with martensitic particle (1 or 2) at two shear-band (I and II) intersection.

The following simplifying assumptions are accepted:

- elastic properties of matrix and martensite are the same;
- shear bands are mutually orthogonal;
- the case of plane strain state is considered;
- the inverse problem is solved, i.e. the position and size of the transforming region is specified *a priori*, and then the condition for PT is determined;
- temperature is homogeneously distributed and does not change during the PT;
- critical driving force k_c is a constant or function of temperature only.

The following properties of a steel are used in the calculations:

- Young's modulus $E = 2.1 \times 10^5$ MPa;
- Poisson ratio $\mu = 0.3$;
- yield stress for matrix $\sigma^{\mathrm{m}}{}_y = 2.5 \times 10^2$ MPa [19];
- yield stress for martensite $\sigma^{\mathrm{n}}{}_y = 8 \times 10^2$ MPa (for simplicity we assume that the yield stress changes instantaneously to the value of phase 2 during PT).

4.1. Displacement-controlled boundary conditions

The following boundary conditions are applied:

- along AB boundary $u_{\mathrm{n}} = 0$, $\tau_{\mathrm{n}} = 0$;
- along CD boundary $u_{\mathrm{n}} = u^*$, $\tau_{\mathrm{n}} = 0$ (u^* is the prescribed normal displacements);
- AC and BD boundaries $\sigma_{\mathrm{n}} = \tau_{\mathrm{n}} = 0$ (free surface).

Here u_{n} is the normal displacement, τ_{n} and σ_{n} are the shear and normal stresses. From crystallography we can define the symmetric transformation left stretch tensor $\mathbf{U}_{\mathrm{t}}$ ($\mathbf{F}_{\mathrm{t}} = \mathbf{R}_{\mathrm{t}} \cdot \mathbf{U}_{\mathrm{t}}$) only. However the problem solution for an isotropic formulation does not depend on the transformation rotation tensor $\mathbf{R}_{\mathrm{t}}$ because we can merge rotation tensors $\mathbf{R}_{\mathrm{t}}$ and $\mathbf{R}_{\mathrm{e}}$ in the total gradient decomposition (2) into one rotation tensor $\mathbf{R}_{\mathrm{et}} = \mathbf{R}_{\mathrm{e}} \cdot \mathbf{R}_{\mathrm{t}}$. Therefore, for the sake of convenience, we can also prescribe the transformation gradient with an arbitrary rotation tensor $\mathbf{R}_{\mathrm{t}}$. For our calculations the transformation gradient is

$$\mathbf{F}_{\mathrm{t}} = \mathbf{I} + \xi(\bar{\mathbf{F}}_{\mathrm{t}} - \mathbf{I}) \quad \xi \in [0, 1]; \quad \bar{\mathbf{F}}_{\mathrm{t}} = \mathbf{I} + \mathbf{kn} \tag{32}$$

and is subdivided into 60 increments. Here $\mathbf{n}$ is the outward unit normal vector to the habit plane and $\mathbf{k}$ is the displacement vector due to transformation. In the local cartesian coordinate system (one axis is directed along vector $\mathbf{n}$, another one is located in the plane of the vectors $\mathbf{n}$ and $\mathbf{k}$ which coincide with the plane of Fig. 2) the transformation gradient $\bar{\mathbf{F}}_{\mathrm{t}}$ has the following components

$$(\bar{\mathbf{F}}_{\mathrm{t}})_{11} = 1, \quad (\bar{\mathbf{F}}_{\mathrm{t}})_{12} = 0.2,$$
$$(\bar{\mathbf{F}}_{\mathrm{t}})_{21} = 0, \quad (\bar{\mathbf{F}}_{\mathrm{t}})_{22} = 1.026, \tag{33}$$

the other components are zero.

As we do not know the direction of the normal $\mathbf{n}$ with respect to the global coordinate system, we will find the most favorable one using the extremum principle (18). We have prescribed four different angles $\alpha = 0$; 45°; 50°; 90° between $\mathbf{n}$ and axis X_2 (Fig. 2). Solving four boundary-value problems for the $u^*_{\max} = 0.24$ and appearance of martensite at the shear-band intersection we have found that the corresponding values of the work integral φ are $\varphi = -36.86$; 22.59; 21.86; −37.06 MPa, respectively. According to the extremum principle (18), the most favorable direction for the vector $\mathbf{n}$ is along one of the shear bands (along the axis X'_2, Fig. 2), since for this direction the work integral $\varphi = 22.59$ has a maximum value. In the following calculation we will use this direction for prescribing the transformation gradient $\bar{\mathbf{F}}_{\mathrm{t}}$. Consequently, the transformation gradient $\bar{\mathbf{F}}_{\mathrm{t}}$ has the components (33) in the local coordinate system in which axes are directed along shear bands.

Four different values of maximal prescribed displacement $u^*_{\max}$ are considered, namely

$$u^*_{\max} = 0.14; \quad 0.19; \quad 0.24; \quad 0.34, \tag{34}$$

which correspond to the following macroscopic tensile strain

$$\varepsilon = U - 1 = u^*_{\max}/h = 0.0047; \quad 0.0063; \quad 0.0080; \quad 0.0133, \tag{35}$$

where $h = 30$ is the initial height of a sample. During the PT the transformation deformation gradient and prescribed displacements grows proportionally to the same parameter ξ,

$$u^*(\xi) = u^*_1 + (u^*_{\max} - u^*_1)\xi, \tag{36}$$

i.e. the transformation deformation gradient grows proportionally to the prescribed displacement. For all cases we start the PT at the boundary condition,

corresponding to macroscopic strain $\varepsilon u_1^*/h = 0.14\%$ when plastic strains appear in shear-band regions. This corresponds to the situation where transformation occurs during the shear-band intersection event. Consideration at higher macroscopic strain gives practically the same results due to perfectly plastic model. Treatment at smaller macroscopic strain suits for stress assisted rather than strain-induced PT.

Note that we do not assume that PT starts at some critical strain. PT occurs when the PT condition (16) is satisfied at given boundary condition and temperature and prescribed macroscopic strain represents boundary condition.

In Fig. 3 the calculated macroscopic stress σ-strain ε diagrams for the sample under consideration and corresponding values of the work integral φ are presented.

Macroscopic axial stress σ is obtained from the problem solution and averaging over the boundary CD. Curves 1–4 correspond to the appearance of martensite at shear-band intersections, curve 5 for deformation without PT (perfect plastic behavior). As described in [4], two opposite factors related to PT are responsible for the shape of the stress–strain diagram:

- appearance of additional transformational deformation modes, namely transformation strain and plastic strain induced by transformation, i.e. transformation induced plasticity (TRIP);
- strengthening due to higher yield stress of the martensitic product.

In curve 2 both these tendencies approximately compensate each other and the material behaves macroscopically similar to the case without PT (curve 5). For curves 3 and 4 additional transformational deformation modes exceed the prescribed strain, and thus macroscopic elastic strain and stress decreases during the transformation. Transformation work for these curves is negative, i.e. stresses resist the growing transformation strain. Martensite is in the elastic state. For curve 1 prescribed strain exceeds transformation strains and strengthening due to the higher yield stress in the martensitic phase leads to higher stresses. Martensite then deforms plastically in the direction of growing transformation shear.

If we know the temperature and k_c, then from the PT criterion (16) we can find the corresponding value of the transformation work φ and choose the prescribed displacement in Fig. 3 at which PT can occur. When the displacement is given, then the transformation work φ can be calculated and from the PT criterion (16) the PT temperature can be defined.

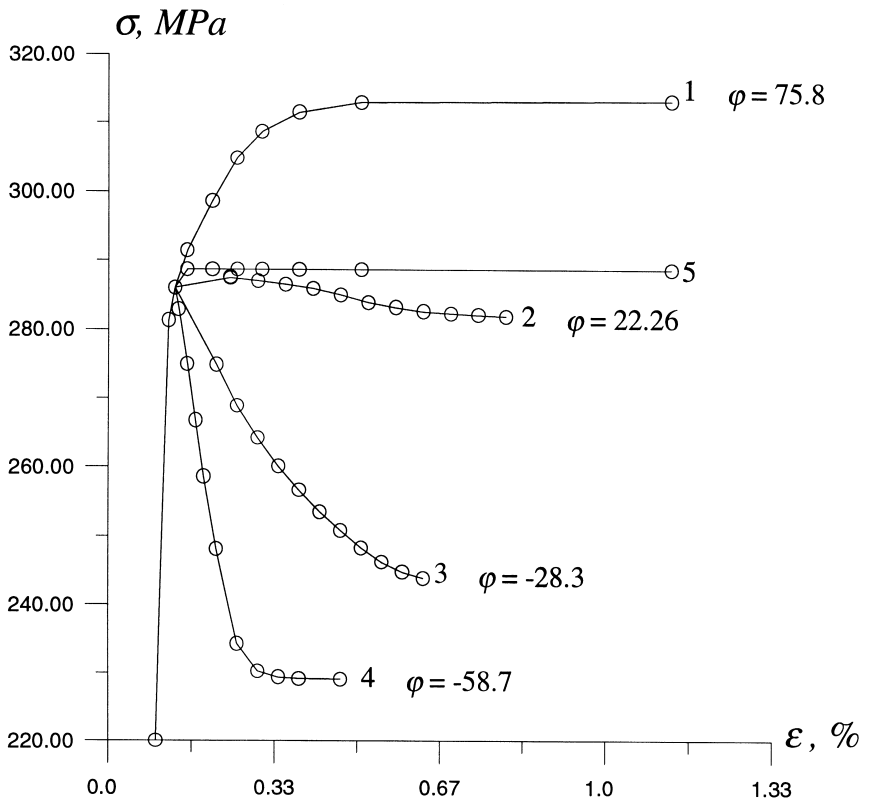

Fig. 3. Relationships between macroscopic axial stress σ and strain ε (at different values of ε after finishing PT) during appearance of martensite at shear band intersection (region 1). 1, work integral $\varphi = 75.8$ MPa; 2, $\varphi = 22.26$ MPa; 3, $\varphi = -28.3$ MPa; 4, $\varphi = -58.7$ MPa; 5, without PT.

As was mentioned in Section 2, the solution without PT (curve 5 in Fig. 3) is always possible, because it satisfies all equations of continuum thermodynamics. To choose which solution—with PT or without PT—will be realized, we can use stability analysis. According to the stability criterion (20), when the σ–ε curve for the solution with PT (curve 1 in Fig. 3) exceeds the σ–ε curve for the solution without PT, the PT would not occur, despite the fact that the local PT criterion can be satisfied. In the opposite case (curves 2–4 in Fig. 3) the deformation process with PT is more stable.

The volume fraction of martensite f_m corresponding to transformation in region 1 is 1/300. As we know the strain increment which is necessary for appearance of such a volume fraction at various φ (or temperatures), we can determine the derivatives $df_m/d\varepsilon$. For the four cases presented in Fig. 3 it is equal to 0.709; 0.529; 0.417 and 0.251 correspondingly.

The results obtained can be reformulated in order to analyze qualitatively the situation with several transformation sites. Let us consider (Fig. 4) the connection in series of four elementary representative volumes presented in Fig. 2. If we neglect elastic strains, then different values of prescribed displacement in Fig. 2 can be obtained by the appearance of martensite at one, two, three or four shear-band intersections in Fig. 4. Let the prescribed strain increment for a system of four elements be 0.333%, i.e. minimum inelastic strain increment in Fig. 2. If martensite appears at each shear-band intersection (four particles), then the work integral and external stress variation will be the same (at neglected elastic strains), as in curve 4 (Fig. 3). When transformation occurs at two intersections and two other elements will be rigid (as external stress is smaller than the yield stress), then the actual prescribed strain for two active elements is 0.666% which corresponds to curve 2 in Fig. 3. For three active intersections the actual prescribed strain increment is 0.444% which is close to 0.49% for curve 3 in Fig. 3. For the transformation at one intersection and three rigid elements the actual prescribed strain is 1.32% which exceeds the value 1.19% for curve 1 in Fig. 3. But even for $\Delta\varepsilon = 1.19\%$ the actual stress exceeds the yield stress for austenite and transformation-free elements cannot be rigid. It is clear that when at least one intersection is not active, then the external stress cannot exceed the macroscopic yield stress. This is in agreement with our results of stability analysis, namely that when the macroscopic stress–strain diagram for the case with PT exceeds the diagram without PT, then PT will not occur. The model with connection in series can be considered as a corroborating example for an extremum principle (20).

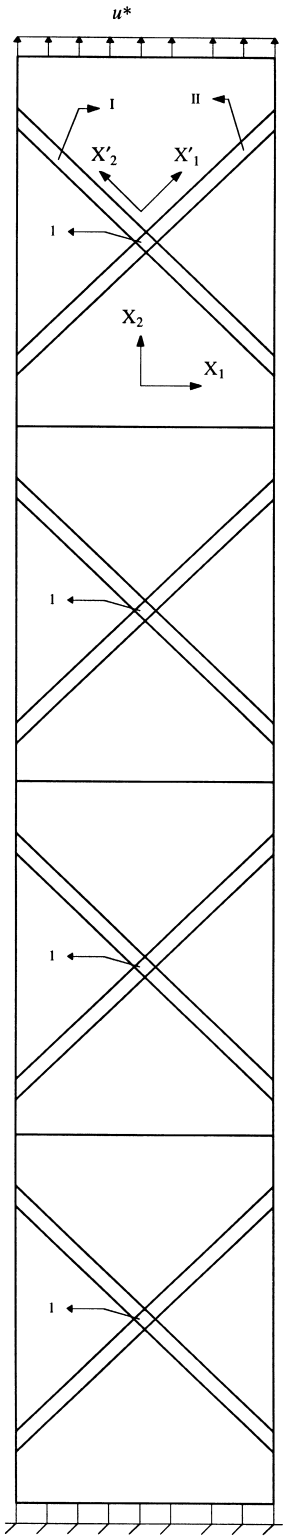

Fig. 4. Connection in series of four representative volumes presented in Fig. 2.

This mechanical model offers further insight as to why transformation need not occur at every shear-band intersection. Even if all intersections are potentially completely equivalent (i.e. materials properties and geometry are the same), stress variation and transformation work depend strongly on the

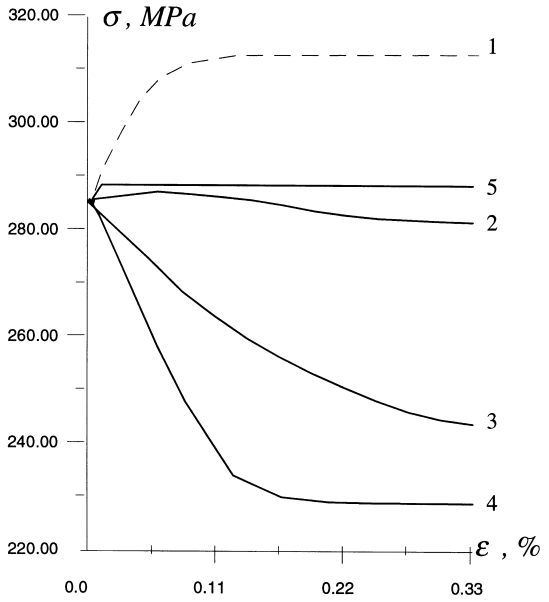

Fig. 5. Macroscopic stress–strain diagram for the system presented in Fig. 4. 1, Appearance of one particle, $\varphi = 75.8$ MPa; 2, two particles, $\varphi = 22.26$ MPa; 3, three particles, $\varphi = -28.3$ MPa; 4, four particles, $\varphi = -58.7$ MPa; 5, without PT.

number of active intersections during the given strain increment. At a given temperature and k_c we can define from the PT criterion (16) the necessary value of the transformation work φ and determine how many intersections in Fig. 5 will transform at the given strain increment. For example, if at the given temperature the transformation work $\varphi = 22.26$ MPa is required for satisfaction of the PT criterion, then two intersections will be active only. If we assume that three or four martensitic particles appear, then PT criterion will be violated. In the framework accepted we cannot say which intersections exactly are active, because they are identical. To choose explicitly active intersections we have to introduce small variation in properties or geometry.

We compare several scenarios of PT process, in particular, how it depends on macroscopic strain increment. Let the necessary transformation work be $\varphi = -58.7$ MPa, i.e. four nucleus can appear (low temperature). Prescribed strain increment grows from zero to final value 0.333%. During this growth material "does not know" the final value of strain increment, perhaps it will be smaller and PT in four elements cannot occur. The first opportunity for PT will be when nucleation occurs at one intersection during the strain increment $0.333/4 = 0.0833\%$, because it leads to the same value of work integral. According to the postulate of realizability [6, 7, 17], as only PT can occur, it will occur. Then stress will grow to the macroscopic yield stress (Fig. 6), and again new nucleus appears at another intersection during the strain increment 0.0833%. Such a process will be repeated four times, i.e. four nuclei appear during the strain increment 0.333%. It is not necessary to compare which of two processes—corresponding to curve 1 or 2—is more stable, because during the strain increment 0.0833% the nucleation at one intersection only is possible.

The same process will take place for all other values of φ: as only PT at one intersection can occur [i.e. the value φ at the smallest strain increment satisfies the PT criterion (16)], it will occur.

It is evident that a possible maximum transformation work at appearance of only one particle corresponds to deformation at maximum macroscopic

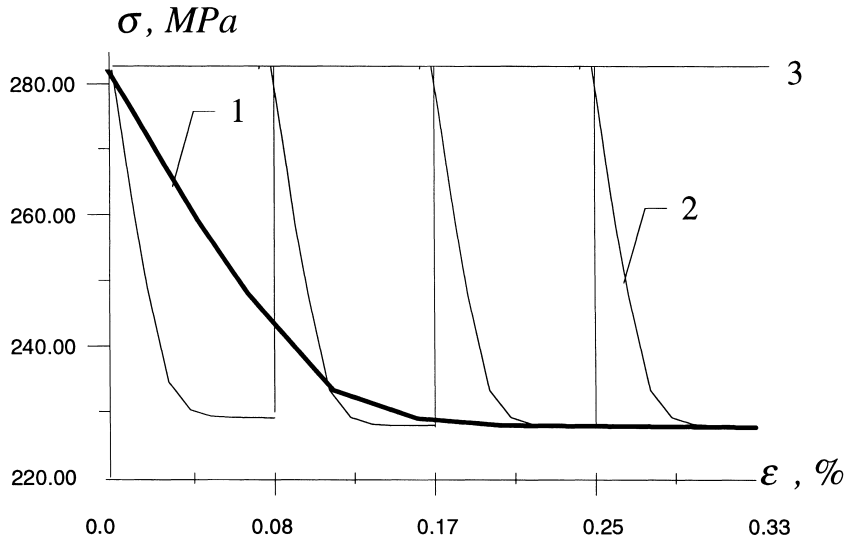

Fig. 6. Macroscopic stress–strain diagram for the system presented in Fig. 4. 1, Four particles appear simultaneously; 2, four particles appear one after another; 3, deformation without PT.

stresses, i.e. at σ equal to the macroscopic yield stress (curve 5 in Fig. 3). From the point of view of stability analysis, deformation with and without the PT is in this case equiprobable. To be sure that deformation with PT will occur, stresses must be infinitesimally smaller than macroscopic yield stress. Thus stability analysis offers a criterion for M_d, the maximum temperature at which PT can be caused by plastic straining.

Some further variants of the occurrence of PT in the model presented in Fig. 2 were compared using the extremum principle (18). For normal displacement $u^*_{max} = 0.19$ on the boundary CD we have also solved the problem with appearance of transformation in volume 2, Fig. 2 (volumes 1 and 2 being equal). The work integral is $\varphi = -42.2$ MPa for this case, i.e. the PT driving force $\bar{X}$ for transformation at the shear-band intersection (volume 1, $\varphi = -28.3$ MPa) is higher than for transformation in volume 2, and, due to extremum principle (19), PT will occur at the same external conditions in volume 1 at the shear-band intersection. Several other locations within one shear band not too close to the free surfaces were checked with the same result. Transformation at an arbitrary place inside the elastic matrix leads to a very low value of φ. Consequently, the shear-band intersection is the most favorable place for transformation consistent with experiment. In the absence of shear-band intersections nucleation will occur in shear band at slightly higher temperature. Similar results are obtained for normal displacement $u^*_{max} = 0.24$ (Fig. 7). When transformation appears simultaneously in region 1 and 2 (large particle), then the PT condition is worse than for transformation at the shear-band intersection, but better than in region 2 (Fig. 7), despite the macroscopic stress being smaller than for transformation in region 2 (allowing for surface energy does not change this conclusion).

To model the growth of particle 1 the problem of subsequent transformation in volume 2 has been solved. However, the value of the work integral φ for volume 2 was much smaller than φ for volume 1 of the initial particle. The reason lies in the higher yield stress of martensite in the transformed volume 1, which increases the resistance to transformation shear. This inhibits martensite growth outside the intersection regions, also consistent with experimental observations.

4.2. Stress-controlled boundary conditions

Let us next consider another type of boundary condition:

•along CD boundary $\sigma_n = \sigma$, $\tau_n = 0$,

i.e. a homogeneously distributed normal stress is prescribed instead of normal displacement. The stress σ is held constant during the increase of transformation strain. This problem models the "creep" test for stress assisted PT, when PT and TRIP occur during the cooling at fixed external stress. The relationship between the work integral φ and applied stress σ is shown in Fig. 8. At $\sigma = 0$, we obtain $\varphi = -89.62$ MPa. Taking a typical value

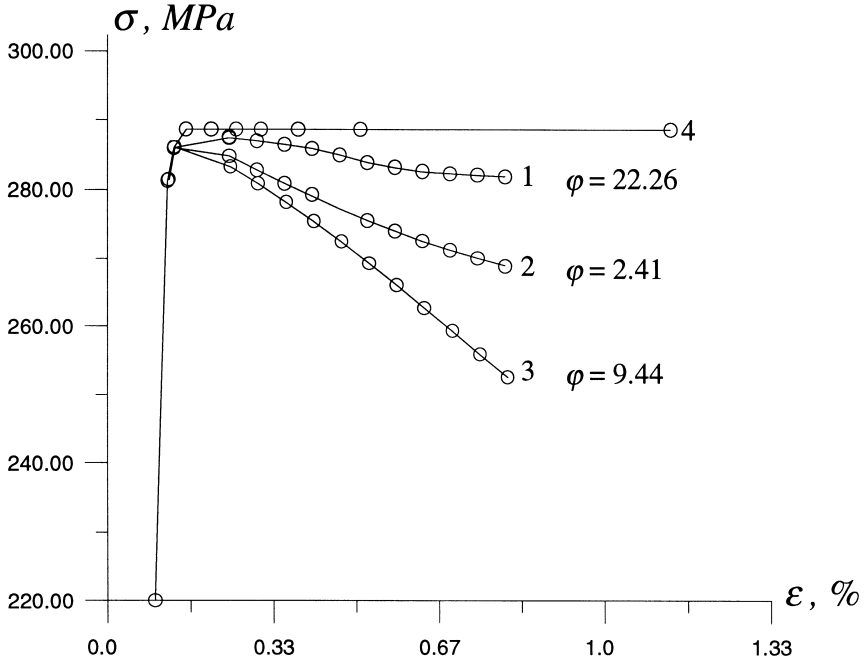

Fig. 7. Relationships between macroscopic axial stress σ and strain ε during appearance of martensite at shear band intersection (region 1), curve 1; at one shear band (region 2), curve 2; and appearance of large particle (region 1 and 2), curve 3. 1, Work integral $\varphi = 22.26$ MPa; 2, $\varphi = 2.41$ MPa; 3, $\varphi = 9.44$ MPa; 4, without PT.

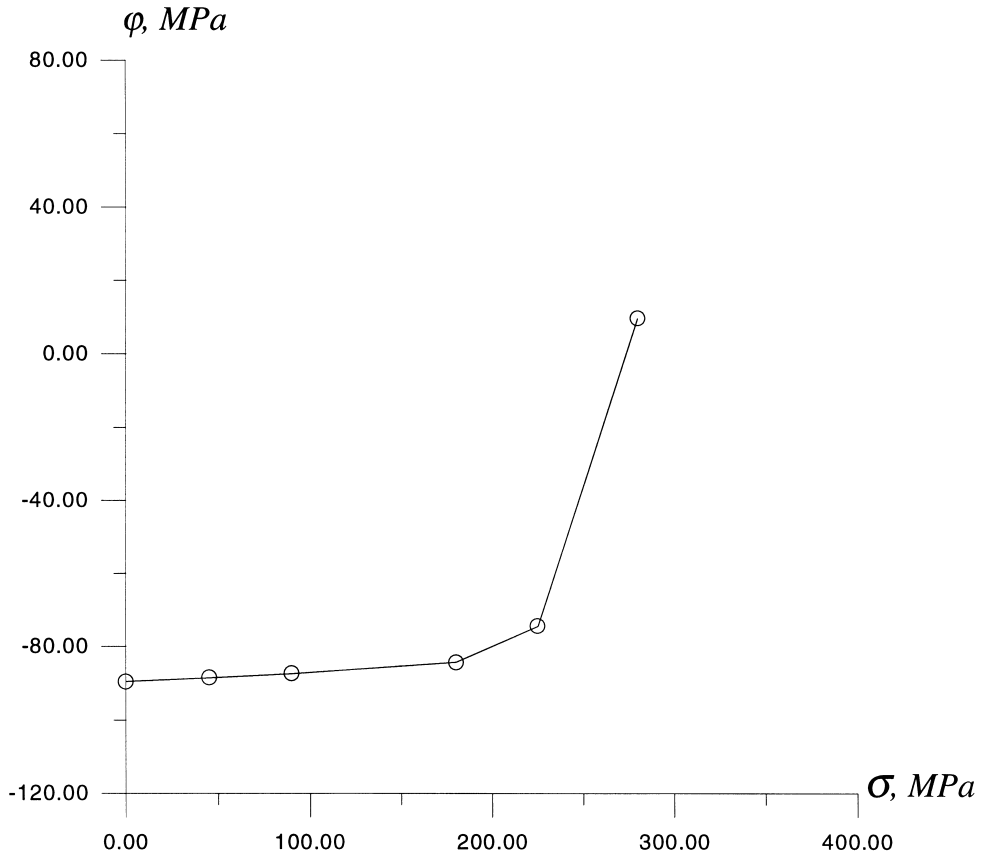

Fig. 8. Relationships between the work integral φ and external axial stress σ.

of $\Delta\psi^{\theta} = -215.12$ MPa at the martensite start temperature M_s, then $k = 125.5$ MPa.

Even without external stresses both matrix and particle deform plastically in order to accommodate a rather large transformation strain. Applied stresses in a range $0 < \sigma < 180$ MPa affect very weakly the transformation work. This can be related to the fact that transformation at shear-band intersections is far from optimal for stress assisted PT (see below). External stresses in this range are not sufficient to deform (together with the transformation strain in the particle) the whole potential shear-band region plastically. Increase in σ leads to extension of the plastic region and practically does not change stress in the intersection, so results are not sensitive to external stress. The negative transformation work produced by internal stresses is much higher than positive work of applied stresses.

In a range $230 < \sigma < 280$ MPa, when σ approaches the macroscopic yield stress, the effect of external stresses on the driving force is very strong. Plastic flow occurs in the whole potential shear-band region and the increase in σ is completely concentrated at the intersection.

For an estimation of the effect of plastic flow in a hard martensitic particle on the driving force for PT, the same problem for an elastic particle (with very high yield stress of martensite) was solved. Results are presented in Fig. 9. At small stress a very large difference between solutions with elasto-plastic (curve 1) and elastic (curve 2) particle is observed. This difference decreases with increasing σ and disappears at $\sigma > 250$ MPa. Results for neglected volumetric transformation strain (curve 3) differ very little from the case with volumetric transformation strain (curve 2).

Calculations demonstrate a strong difference between PT conditions for displacement and stress controlled boundary conditions. For the prescribed displacement the increase of particle size leads to a reduction of macroscopic stresses σ and the driving force for PT. For the fixed external stresses, the increase in particle size increases the macroscopic axial strain and the transformation work. Maximum transformation work will be when the whole band transforms into the martensitic state without plastic straining and is equal to the total work of applied stress. If transformation under prescribed stress $\sigma = 280$ appears in region 1 (Fig. 10), the transformation work is $\varphi = 9$ MPa. As in the case with prescribed displacements, the work integral decreases significantly $\varphi = -73$ MPa for PT in the region 2 (at growth of particle 1) due to the

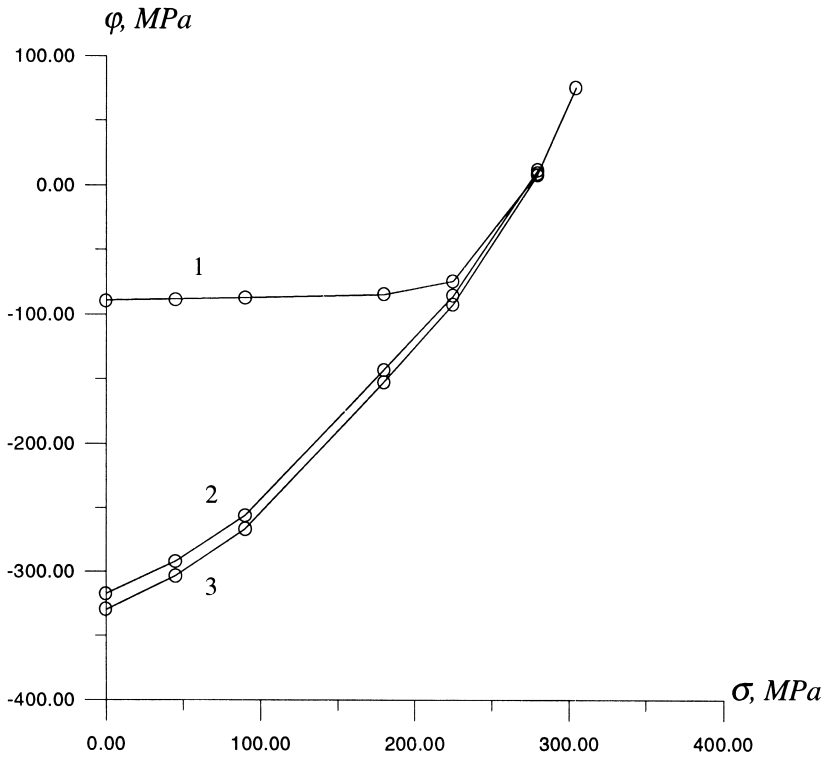

Fig. 9. Relationships between the work integral φ and external axial stress σ. 1, Elastoplastic martensite; 2, elastic martensite; 3, elastoplastic martensite with transformation shear strain only.

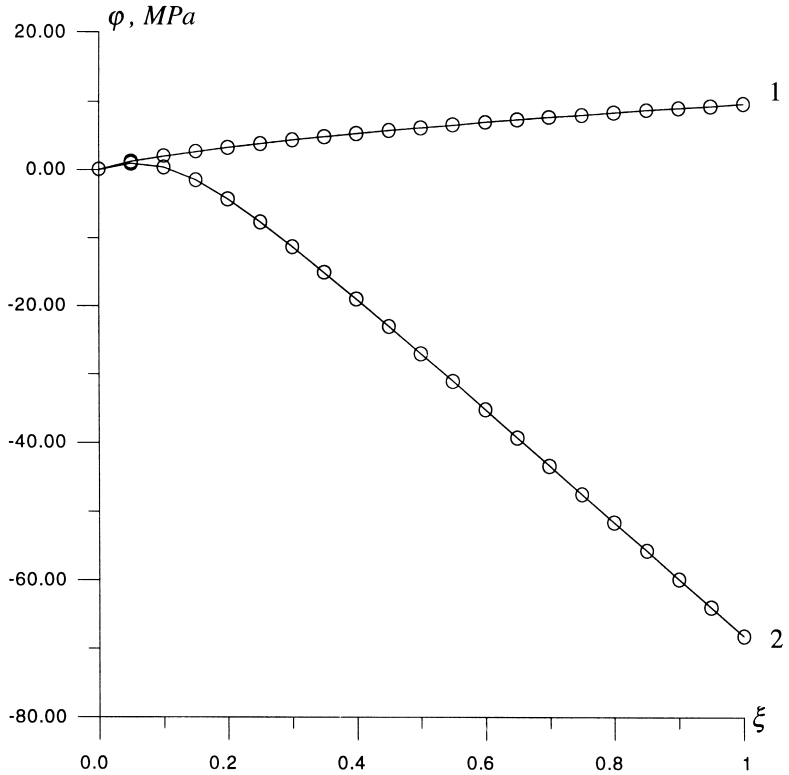

Fig. 10. Work integral φ as function of the internal order ξ. 1, Martensite at two shear-band intersections; 2, second particle (or particle growth).

necessity to deform the high strength martensite in region 1.

It is then possible to explain qualitatively why transformation at shear-band intersections occurs more readily during plastic deformation (i.e. at prescribed strain which exceeds the elastic limit) than under applied stress on cooling after the plastic deformation [1]. Assume the value $\varphi = -28.85$ MPa is required for PT. Then PT occurs at the prescribed strain 0.66% (Fig. 3, curve 3) and the stress after transformation is 248 MPa. At such a value of prescribed stress $\varphi = -39$ MPa, i.e. additional cooling is necessary for the transformation at another intersection. On cooling the yield stress increases, i.e. the ratio of applied stress to yield stress decreases. In this case the work integral decreases significantly as well (Fig. 8).

5. CONCLUDING REMARKS

In this paper a numerical solution of the problem of transformation at shear bands is considered, based on the mesoscopic continuum thermodynamic model of martensitic PT developed in papers [5–7]. By this model, the location and morphology of transformation in a heterogeneous plastic medium corresponds to the maximum transformation work during the whole PT process. Stress variation during the PT makes the transformation work a complex functional of boundary conditions, material properties and transformation deformation gradient. It is very difficult to predict beforehand how these parameters affect the transformation work, and numerical solutions are essential to provide useful insights.

It is demonstrated that for strain-induced transformation at shear-band intersections the transformation work is maximal in comparison with other possible locations. Further growth beyond the intersection is inhibited, because the transformation work decreases significantly and transformation at other shear-band intersections is favored. Transformation work depends strongly on the number of active shear-band intersections at the prescribed macroscopic strain increment. This favors sequential transformation at multiple intersections, even when the intersections are completely equivalent. At a given temperature, the necessary transformation work can be determined from the PT criterion, and the number of active intersections can be obtained using the numerical solution. PT is favored during the intersection event rather than after intersection and cooling at fixed stress.

All four experimental observations enumerated in the Introduction can be at least qualitatively described in the framework of continuum thermomechanics without detailed physical mechanisms. A connection to microscopic theory has been made with the approximation that the critical nucleus thickness is equal to that of shear band. While more explicit treatment of capillarity, prestrain and embryo growth path will provide further insights, this study demonstrates that many observed features are consistent with more macroscopic mechanical considerations. The relevance of stability analysis for strain-induced PT has been explored. According to the stability criterion (20), when the σ–ε curve for the solution with PT (curve 1 in Fig. 3) exceeds the σ–ε curve for the solution without PT, the PT will not occur, even when the local PT criterion can be satisfied. Such a situation can occur at high temperature when a large transformation work is required for PT. This offers a possible criterion for the M_d temperature.

Calculations also demonstrate a large difference between PT conditions for displacement and stress controlled boundary conditions. For a given fixed external stresses martensite growth increases the macroscopic axial strain and the transformation work, favoring growth beyond the intersection region, in contrast to the restricted growth predicted under displacement control.

Acknowledgements—V.I.L. and A.V.I. gratefully acknowledge the support of the Volkswagen Foundation, grant I/70283 and discussions with Professor E. Stein. Research on martensitic transformation at Northwestern University is sponsored by the National Science Foundation under Grant DMR9500122.

REFERENCES

1. Olson, G.B. and Cohen, M., *J. Less-Common Metals*, 1972, **28**, 107.
2. Olson, G. B., in *Deformation, Processing and Structure*, ed. G. Krauss. ASM International, Warrendale, PA, 1984, p. 391.
3. Olson, G.B. and Cohen, M., *Metall. Trans.*, 1975, **6A**, 791.
4. Stringfellow, R.G., Parks, D.M. and Olson, G.B., *Acta metall. mater.*, 1992, **40**, 1703.
5. Levitas, V.I., *J. Phys. IV, Colloque C1*, 1996, **6**, 55.
6. Levitas, V. I., *J. Mech. Phys. Solids Part I*, 1997, **45**, 923, *Part II*, **45**, 1203.
7. Levitas, V.I., *Int. J. Solids Struct.*, 1998, **35**, 889.
8. Idesman, A. V., Levitas, V. I. and Stein, E., in *Proc. 5th Int. Conf. on Num. Meth. in Plasticity (COMPLAS 5), Barcelona*, ed. E. Onate *et al.*, Pineridge Press, Swansea, 1997, p. 1323.
9. Idesman, A.V., Levitas, V.I. and Stein, E., *Comput. Mater. Sci.*, 1997, **9**, 64.
10. Levitas V.I, Idesman, A.V. and Stein E. Int. J. Solids Struct. 1998 **35,** 855.
11. Idesman, A.V. and Levitas, V.I., *Comput. Meth. Appl. Mech. Engng*, 1995, **126**, 39.
12. Levitas, V. I., 1996. *Large Deformation of Materials with Complex Rheological Properties at Normal and High Pressure*. Nova Science, New York.
13. Olson, G.B. and Cohen, M., *Metall. Trans.*, 1976, **7A**, 1897.
14. Olson, G. B. and Cohen, M. 1986. in *Dislocations in Solids*. ed. Nabarro FRN. North-Holland, Amsterdam. Vol. 7. Chap. 37. p. 295.
15. Ghosh, G. and Olson, G.B., *Acta metall. mater.*, 1994, **42**, 3361.
16. Ghosh, G. and Olson, G.B., *Acta metall. mater.*, 1994, **42**, 3371.

17. Levitas, V.I., *Int. J. Engng Sci.*, 1995, **33**, 921.
18. Simo, J.C. and Miehe, C., *Comput. Meth. Appl. Mech. Engng*, 1992, **98**, 41.
19. Marketz, F. and Fischer, F.D., *Comput. Mater. Sci.*, 1994, **3**, 307.

APPENDIX

Finite element solution algorithm

1. Initialization at t_n. Data structure:

Variables at quadrature points

$\{p, \mathbf{s}, q, I_1(\mathbf{B}_e), dev\mathbf{B}_e, \mathbf{U}_p, \mathbf{R}_e\}_n$

Initial conditions for displacement vector at nodal points $\{u\}_{n+1}=0$

Initial nodal coordinates $\{x\}_n$

Transformation gradient increment $\{\Delta\mathbf{F}_t\}_{n+1}$ and boundary conditions

2. Let $\{u\}^k_{n+1}$ be solution at the k-iteration.

2.1 Update nodal coordinates

$\{x\}^k_{n+1}=\{x\}_n+\{u\}^k_{n+1}$

2.2 Compute $\{\mathbf{F},\mathbf{d},\mathbf{d}_t,\bar{\mathbf{W}}\}^k_{n+1}$ at quadrature points [equation $(2)_1$, $(3)_1$, $(4)_2$, $(5)_{2,3}$]

2.3 Compute at quadrature points $\{\mathbf{s},q,\mathbf{U}_p\}^k_{n+1}$ by numerical integration (defining rate of this parameters from equations (29), (14) and $(7)_2$, $(4)_1$, and $\{p,I_1(\mathbf{B}_e), dev\mathbf{B}_e, \mathbf{R}_e\}^k_{n+1}$, using the equations (30), (31), (6) and $(2)_3$

2.4 Compute residuals

$$\{\Psi\}^k_{n+1}=\{f\}^k_{n+1}-\int_{V^k_{n+1}}[B]^k_{n+1}\{T\}^k_{n+1}\,dV$$

($\{f\}^k_{n+1}$ is the standard finite element load vector, $[B]^k_{n+1}$ is standard B-matrix for finite elements with updated coordinates $\{x\}^k_{n+1}$).

IF $\|\{\Psi\}^k_{n+1}\| <$ TOL GO TO 4

3. Solve system $[K]\{\Delta u\}^k_{n+1}=\gamma\{\Psi\}^k_{n+1}$, $[K]$ is stiffness matrix, $\gamma\in[0,1]$

Update $\{u\}^{k+1}_{n+1}=\{u\}^k_{n+1}\}+\{\Delta u\}^k_{n+1}$

Set $k=k+1$ and GO TO 2

4. Update data structure

$\{p, \mathbf{s}, q, I_1(\mathbf{B}_e), dev\mathbf{B}_e, \mathbf{U}_p, \mathbf{R}_e\}_{n+1}=$

$\{p, \mathbf{s}, q, I_1(\mathbf{B}_e), dev\mathbf{B}_e, \mathbf{U}_p, \mathbf{R}_e\}^k_{n+1}$

Update nodal coordinates $\{x\}_{n+1}=\{x\}^k_{n+1}$.